

Photoproduction of isolated photon and jet at the DESY HERA

Andrzej Zembrzuski, Maria Krawczyk

*Institute of Theoretical Physics, Warsaw University,
ul. Hoża 69, 00-681 Warsaw, Poland*

Abstract

The next-to-leading order (NLO) QCD calculation for the isolated photon and isolated photon plus jet photoproduction at the ep collider DESY HERA is presented. The predictions for the isolated photon with no restrictions imposed on the jet are compared with the previous ones obtained in the small cone approximation, and the differences are found to be below 2%. The theoretical uncertainties in the cross section of the photoproduction of the photon plus jet are discussed. A short comparison with the new preliminary H1 data and with the NLO predictions of Fontannaz et al. is also presented.

1 Introduction

In the previous papers [1, 2] we have presented the next-to-leading order QCD calculation (NLO) for the photoproduction of a photon with large transverse momentum, so called prompt photon, at the ep collider HERA. We have also shown the leading order (LO) predictions for the prompt photon and a jet production [2]¹.

For comparison with experimental data, the final photon was considered in [1, 2] as an isolated one, i.e. the hadronic energy within some cone around the photon was restricted. We introduced the isolation in an approximated way with the assumption that the momenta of partons inside the isolation cone were almost collinear with the photon momentum (small cone approximation).

In this paper we study in NLO the photoproduction of both the isolated (prompt) photon and isolated (prompt) photon plus a jet without the small cone approximation. Since the numerical differences between the present calculation and the previous approximated one are found to be very small for the photoproduction of the isolated photon, we focus our attention mainly on the NLO predictions for the isolated photon observed in the final state together with a jet, see fig. 1.

The photoproduction is a process in which a real or almost real photon is collided with another particle in order to produce some final state (for a recent reviews see [3, 4, 5]). In an electron-proton scattering the photoproduction corresponds to the small virtuality of the exchanged photon, Q^2 , say $Q^2 \lesssim 1 \text{ GeV}^2$ [6, 7, 8, 9, 10]. In such a case this almost real photon colliding with the proton may lead for instance to a production of jets or particles with large transverse momenta.

The photoproduction of the prompt photon in the ep or γp collision have been studied theoretically (for a non-isolated final photon) since 1969 [11]-[24]. Then the NLO predictions for the isolated photon have been presented by various authors [25, 1, 26, 2]. The photoproduction of the isolated photon and a jet at HERA have been calculated in NLO by Gordon [27] and Fontannaz, Guillet and Heinrich [28]. There is also a NLO calculation for the isolated photon and isolated photon plus a jet production in

¹A rough estimation of NLO predictions for the photon plus jet production was given in [1].

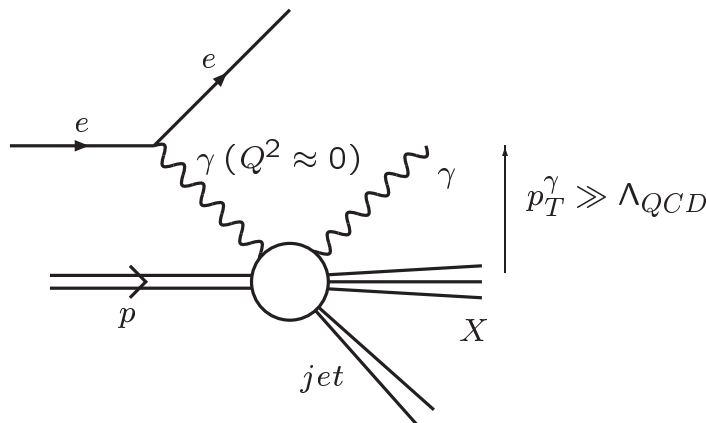


Figure 1: *The $ep \rightarrow e\gamma \text{ jet } X$ photoproduction.*

the deep inelastic scattering ($Q^2 \gg 1 \text{ GeV}^2$) [29], which is in many theoretical aspects close to the calculations for the corresponding photoproduction events.

The photoproduction of isolated photons without and with additional jets has been measured at the HERA collider by the ZEUS [6, 7, 8, 9] and H1 [30, 10] Collaborations. In general, the data are in reasonably agreement with NLO predictions. Nevertheless, none of theoretical predictions as well as Monte Carlo simulations give sufficiently good description of the ZEUS data [7, 8] (see also [31]) for the isolated photon at negative photon rapidities (η_γ). Some discrepancies between NLO [28] and data are also seen for the preliminary H1 data [10], mainly at $\eta_\gamma > 0.6$ and $x_\gamma < 0.5$.

In the paper [9] the ZEUS Collaboration has considered in Monte Carlo simulations the intrinsic transverse momentum of partons in the proton in photoproduction events containing the prompt photon plus jet, and the effective intrinsic transverse momentum was found to be $\langle k_T \rangle = 1.69 \pm 0.18_{-0.20}^{+0.18} \text{ GeV}$. On the other hand, no need for the intrinsic transverse momentum in the proton was reported in [28].

In our analysis the intrinsic transverse momentum is not included, since we think that the measured $\langle k_T \rangle$ is not due to the transverse momenta of partons inside the proton, but it describes effectively higher order emissions or multiple interactions.

The paper is organized as follows. First, in sec 2 the processes contributing in NLO and the general formula for the cross section are shortly presented. The isolation cuts and the jet definition are introduced in sec. 3. In sec. 4 the slicing of the three body phase space is discussed, and some other calculation details and inputs are given in sec. 5. The predictions for the $ep \rightarrow e\gamma X$ process are given in sec. 6. The results for the $ep \rightarrow e\gamma \text{ jet } X$ process, discussion of theoretical uncertainties, and comparison with the new preliminary H1 data, as well as with the predictions of Fontannaz et al. [28] are presented in sec. 7. A short summary is given in sec. 8.

2 Cross section

In our previous papers [1, 2] we have discussed the NLO calculation of the cross section of the isolated photon production in the ep collision. The set of contributing diagrams was different than in NLO calculations of other authors [25, 26, 27, 28], since we assumed that parton densities in the photon were of order $\mathcal{O}(\alpha)$, while in the cited papers they were assumed to be of order $\mathcal{O}(\alpha/\alpha_S)$.

The parton densities inside the photon are proportional to the electromagnetic coupling, α , and to the logarithm of the energy scale μ at which the densities are probed, $\ln(\mu^2/\Lambda_{QCD}^2)$ [32, 33, 34]. This logarithm is formally proportional to $1/\alpha_S(\mu^2)$ but it originate from the pure electromagnetic process, $\gamma \rightarrow q\bar{q}$, with no strong interactions, and therefore the parton densities in the photon should be treated as quantities of order $\mathcal{O}(\alpha)$, and not $\mathcal{O}(\alpha/\alpha_S)$. This different treatment of parton densities leads to different set of diagrams in NLO calculations involving resolved photons, and to some moderate differences in numerical predictions in comparison with predictions of other authors [2].

²We define the scale μ in sec. 5.

In the present calculation we take into account the same set of contributing partonic processes as it was taken in [2], namely: the Born diagram ($\gamma q \rightarrow \gamma q$) together with QCD corrections, the box diagram ($\gamma g \rightarrow \gamma g$) [35], processes with the resolved initial or final photon, and processes with resolved both the initial and final photon. The general formula for the differential cross section for the $ep \rightarrow e\gamma X$ (or $ep \rightarrow e\gamma \text{ jet } X$) photoproduction is:

$$d\sigma^{ep \rightarrow e\gamma(jet)X} = \int G_{\gamma/e}(y) d\sigma^{\gamma p \rightarrow \gamma(jet)X} dy, \quad (1)$$

and

$$d\sigma^{\gamma p \rightarrow \gamma(jet)X} = \sum_{a=\gamma, q, \bar{q}, g} \int dx_\gamma \sum_{b=q, \bar{q}, g} \int dx \sum_{c=\gamma, q, \bar{q}, g} \int \frac{dz}{z^2} f_{a/\gamma}(x_\gamma, \mu^2) \cdot f_{b/p}(x, \mu^2) D_{\gamma/c}(z, \mu^2) d\sigma^{ab \rightarrow cd_1} + \sum_{b=q, \bar{q}, g} \int dx f_{b/p}(x, \mu^2) d\sigma^{\gamma b \rightarrow \gamma d_1 d_2}, \quad (2)$$

where $ab \rightarrow cd_1$ and $\gamma b \rightarrow \gamma d_1 d_2$ are the partonic processes.

The eq. 1 is the Weizsäcker-Williams approximation [36, 37] (see also e.g. [38, 39, 5]) with the flux of the real photons emitted from the electron given by $G_{\gamma/e}(y)$, where y is the fraction of the initial electron momentum carried by the photon. The functions $f_{a/\gamma}$, $f_{b/p}$, and $D_{\gamma/c}$ stand for parton distributions in the photon and proton, and a fragmentation function into the photon, respectively. For the direct initial ($a = \gamma$) or final ($c = \gamma$) photon the corresponding distributions are replaced by the δ -functions: $f_{a/\gamma} = \delta(x_\gamma - 1)$ or $D_{\gamma/c} = \delta(z - 1)$. The longitudinal-momentum fractions in the photon and proton parton densities, and in the fragmentation functions are denoted as x_γ , x , and z , respectively, while μ stands for the factorization/renormalization scale.

The calculation of the partonic cross sections, $d\sigma^{\gamma b \rightarrow \gamma d_1 d_2}$, involve isolation restrictions and other kinematic cuts, as used in corresponding experimental analyses.

3 Isolation cut and jet definition

The NLO calculation includes partonic processes with two ($2 \rightarrow 2$) or three ($2 \rightarrow 3$) particles in the final state:

$$ab \rightarrow cd_1(d_2), \quad (3)$$

where a is the photon or a parton originating from the photon, b is a parton from the proton, c stand for the final photon or a parton which decay into the photon in the fragmentation process, and d_i are quarks and/or gluons. The outgoing partons d_i are not observed in the final state - they recombine into colorless hadronic jets.

In experimental analyses the final photon is required to be isolated, i.e the transverse energy of hadrons inside a cone of radius R around the photon is assumed to be less than ϵ times the photon transverse energy,

$$\sum_{hadrons} E_T^{hadron} < \epsilon E_T^\gamma, \quad (4)$$

where ϵ is a small parameter. The cone is defined in the rapidity and azimuthal-angle phase space,

$$\sqrt{(\eta_{hadron} - \eta_\gamma)^2 + (\phi_{hadron} - \phi_\gamma)^2} < R. \quad (5)$$

The some isolation restriction is taken into account in theoretical parton-level predictions, where the sum in eq. (4) runs over c -parton remnant and over d_i -partons, if they are inside the cone (5). In the present calculation we take $R = 1$ and $\epsilon = 0.1$, as in the H1 and ZEUS Collaborations' analyses.

In the partonic $2 \rightarrow 2$ processes with a direct final photon ($c = \gamma$),

$$ab \rightarrow \gamma d_1, \quad (6)$$

the photon is isolated by definition. If the final photon comes from the fragmentation process ($c \neq \gamma$),

$$ab \rightarrow cd_1, \quad (7)$$

it is isolated for the momentum fraction $z > 1/(1 + \epsilon)$, and this cut is used in an integration in eq. (2). An inclusion of the isolation in the partonic cross sections for $2 \rightarrow 3$ processes,

$$\gamma b \rightarrow \gamma d_1 d_2, \quad (8)$$

is more complicated, since one needs to restrict the final momenta of two partons (eq. 4, 5), and to care about a cancellation and factorization of singularities, as described in the next section.

For $2 \rightarrow 2$ processes only one jet appears, and it originates from the d_1 -parton. The jet's transverse energy, rapidity, and azimuthal angle are assumed equal to the transverse energy, rapidity, and azimuthal angle of the d_1 -parton.

Two partons, d_1 and d_2 , produced in the $2 \rightarrow 3$ subprocess may lead to two separate jets or they may form one jet. A number of jets in the final state depends on the jet definition. In this paper the inclusive k_T -jet finding algorithm [40] is employed.

Since in NLO calculation we deal with no more than two partons forming a jet/jets, the algorithm becomes very simple. If the distance between the partons, R_{12} , defined as

$$R_{12} = \sqrt{(\eta^{d_1} - \eta^{d_2})^2 + (\phi^{d_1} - \phi^{d_2})^2}, \quad (9)$$

is larger than an arbitrary parameter R_J , then two separate jets arise with transverse energies, rapidities, and azimuthal angles of the d_i -partons:

$$E_T^{jet_i} = E_T^{d_i}, \quad \eta^{jet_i} = \eta^{d_i}, \quad \phi^{jet_i} = \phi^{d_i}, \quad i = 1, 2. \quad (10)$$

For $R_{12} < R_J$ the d_i -partons are treated as ingredients of one jet with

$$E_T^{jet} = E_T^{d_1} + E_T^{d_2}, \quad (11)$$

$$\eta^{jet} = (E_T^{d_1} \eta^{d_1} + E_T^{d_2} \eta^{d_2}) / E_T^{jet}, \quad (12)$$

$$\phi^{jet} = (E_T^{d_1} \phi^{d_1} + E_T^{d_2} \phi^{d_2}) / E_T^{jet}. \quad (13)$$

Following experimental analyses, $R_J = 1$ will be used in numerical calculations.

4 Phase-space integration

To obtain predictions, one needs to perform an integration over four-momentum of at least one final particle, since unintegrated partonic cross sections contain $\delta^{(4)}$ -functions. In case of $2 \rightarrow 2$ processes with no virtual gluon exchange this integration is straightforward, and will not be discussed.

There are three types of diagrams giving NLO corrections to the Born process, namely: $\gamma q \rightarrow \gamma qg$ (real gluon emission), $\gamma g \rightarrow \gamma q\bar{q}$, and the process $\gamma q \xrightarrow{g^*} \gamma q$ with a virtual gluon exchange. The cross sections of the above processes contain infrared singularities. For numerical integration over momenta of final particles, one needs to isolate these singularities [26, 27]. Like in earlier calculations for the $ep \rightarrow e\gamma(\text{jet})X$ reaction [26, 27, 28], also in the present one the phase space is sliced into a few parts.

Let us assume that θ_{ji} is an angle between the momentum of d_i parton and the momentum of an initial particle j , where $j = e, p$. Let us also define the distance, $R_{\gamma i}$, between the d_i parton and the final photon:

$$R_{\gamma i} = \sqrt{(\eta_{d_i} - \eta_\gamma)^2 + (\phi_{d_i} - \phi_\gamma)^2}. \quad (14)$$

We define the parts of the phase space in the following way:

- Part 1. In the first part the variable w (see Appendix A) is assumed in the range $w_{cut} \leq w \leq 1$, where w_{cut} is an arbitrary parameter close to 1: $0 < 1 - w_{cut} \ll 1$. This region of the phase space contains all types of NLO corrections: virtual gluon exchange, real gluon emission, and the process $\gamma g \rightarrow \gamma q\bar{q}$. The virtual gluon exchange is a $2 \rightarrow 2$ process, while the other ones are of $2 \rightarrow 3$. However, for w close to 1, $w_{cut} < w \leq 1$, the two final partons in the $2 \rightarrow 3$ processes are almost collinear or/and one of the final partons is soft. For w_{cut} sufficiently close to 1 the kinematics of the $2 \rightarrow 3$ processes is almost the same as in the $2 \rightarrow 2$ case:

$$\gamma b \rightarrow \gamma d \quad , \quad d \equiv d_1 + d_2, \quad (15)$$

where the “particle” d has four-momentum equal to the sum of four-momenta of the d_i -partons, and its mass is almost zero. In this case the final photon is isolated and the jet can be identified with the d -“particle”.

The other parts of the phase space, parts 2-5 described below, are defined for $w < w_{cut}$, and contain only $2 \rightarrow 3$ processes.

- Part 2. In this region $w < w_{cut}$ and $\theta_{cut} > \min(\theta_{e1}, \theta_{e2})$, where θ_{cut} is a small arbitrary parameter, $\theta_{cut} \ll 1$. Here, one of the final partons has the momentum almost collinear to the momentum of the initial electron and it, for sufficiently small θ_{cut} , does not enter the isolation cone around the final photon, and does not enter the cone defining the jet. The second parton has a large transverse momentum balancing the photon transverse momentum, so the final photon is isolated, and the jet consists (on the partonic level) of only this very parton.

- Part 3. Here $w < w_{cut}$ and $\theta_{cut} > \min(\theta_{p1}, \theta_{p2})$. One of the final partons has momentum almost collinear to the momentum of the proton, and, like in part 2, the final photon is isolated and the high- E_T jet originates from the second parton alone.

- Part 4. Here $w < w_{cut}$ and $R_{cut} > \min(R_{\gamma 1}, R_{\gamma 2})$, where R_{cut} is a small parameter, $R_{cut} \ll 1$. In this case one of the final partons, say d_1 -parton, is almost collinear to the final photon and the photon is isolated if $E_T^{d_1} < \epsilon E_T^\gamma$. This d_1 -parton does not contribute to the jet.

- Part 5. The last part is defined as the region in which there are no collinear configurations: $w < w_{cut}$, $\theta_{cut} < \min(\theta_{e1}, \theta_{e2})$, $\theta_{cut} < \min(\theta_{p1}, \theta_{p2})$, and $R_{cut} < \min(R_{\gamma 1}, R_{\gamma 2})$.

In numerical calculations we apply in part 1 the formulae integrated over four-momenta of the final partons and virtual gluons [17, 41], namely the eqs. (24) and (37) from ref. [17]. In these formulae all the soft gluon singularities present in the virtual gluon and real gluon corrections are canceled, and all the collinear singularities are factorized into the parton densities.

Parts 2-5 contain no contribution from the virtual gluon exchange, and no soft gluon singularities. Analytical expressions for cross sections corresponding to parts 2, 3, and 4 are given in the Appendix B. All the collinear singularities appearing in the calculations are factorized into parton densities in the photon (part 2), proton (part 3), and into fragmentation functions (part 4).

The cross section in part 5 has no singularities at all, and one can perform an exact numerical integration over final four-momenta in any kinematic range, including isolation restrictions and other cuts. For this purpose we use the squared matrix element given in eqs. (36) (with $\varepsilon = 0$) in ref. [17].

We assume that the cut-off angle θ_{cut} is defined in the centre of mass of the initial photon and the initial parton. The predictions should not depend on a choice of unphysical cut-off parameters, $1 - w_{cut}$, θ_{cut} and R_{cut} , if they are small enough. On the other hand, they can not be too small, since very low values lead to large numerical errors. The results presented in secs. 6 and 7 are obtained with $1 - w_{cut} = \theta_{cut} = R_{cut} = 0.01$. We have checked that the change of the predictions due to the variation of these parameters is negligible, below 1%, if they are taken in the range $10^{-4} \leq 1 - w_{cut} \leq 0.03$, $10^{-4} \leq \theta_{cut} \leq 0.05$ and $10^{-4} \leq R_{cut} \leq 0.05$.

5 Other calculation details

Our NLO calculations are performed in the $\overline{\text{MS}}$ scheme. The factorization/renormalization scales in parton densities and fragmentation functions are assumed equal to the renormalization scale in the strong coupling constant and are denoted as μ . As a reference μ equal to the transverse momentum (transverse energy) of the final photon is taken, $\mu = p_T^\gamma = E_T^\gamma$. For comparison $\mu = E_T^\gamma/2$ and $\mu = 2E_T^\gamma$ will be also considered.

The two-loop strong coupling constant,

$$\alpha_S(\mu^2) = \frac{12\pi}{(33 - 2N_f) \ln(\mu^2/\Lambda^2)} \left[1 - \frac{6(153 - 19N_f) \ln[\ln(\mu^2/\Lambda^2)]}{(33 - 2N_f)^2 \ln(\mu^2/\Lambda^2)} \right], \quad (16)$$

is used with the QCD parameter $\Lambda=0.386, 0.332$ and 0.230 GeV for the number of active massless flavours $N_f=3, 4$ and 5 , respectively. In LO we use one-loop α_S with

$\Lambda=0.123$ GeV and $N_f=4$. The above Λ values are obtained by us from the world average of α_S at the scale M_Z [42]:

$$\overline{\alpha_S}(M_Z) = 0.1183 \pm 0.0027. \quad (17)$$

To minimize theoretical and experimental uncertainties, $\overline{\alpha_S}(M_Z)$ was determined from precise data based on NNLO analyses only. The data given at scales different than M_Z were extrapolated to the M_Z scale using the four-loop coupling. Although we use one- and two-loop expressions, we have applied (17) as the best estimation of the true value of $\alpha_S(M_Z)$.

In numerical calculations we take the Glück-Reya-Vogt (GRV) LO and NLO parton densities in the proton [43] and photon [44], and the NLO GRV fragmentation functions [45]. For comparison we also use other parametrizations, namely Martin-Roberts-Stirling-Thorne (MRST2002) [46], CTEQ6 [47], Aurenche-Guillet-Fontannaz (AFG) [48] and (AFG02) [49], Gordon-Storow (GS) [51], Cornet-Jankowski-Krawczyk-Lorca (CJKL) [52], Duke-Owens (DO) [15], and Bourhis-Fontannaz-Guillet (BFG) [53].

The initial electron and proton energies at the HERA collider are assumed equal to $E_e = 27.6$ GeV and $E_p = 920$ GeV, respectively. In the Weizsäcker-Williams approximation [36, 37] the photon spectrum in the electron is taken in the form [39]:

$$G_{\gamma/e}(y) = \frac{\alpha}{2\pi} \left\{ \frac{1 + (1-y)^2}{y} \ln \left[\frac{Q_{max}^2(1-y)}{m_e^2 y^2} \right] - \frac{2}{y} \left(1 - y - \frac{m_e^2 y^2}{Q_{max}^2} \right) \right\}, \quad (18)$$

with the maximal virtuality $Q_{max}^2 = 1$ GeV. The above formula describes the spectrum of equivalent real (transversally polarized) photons. We neglect longitudinally polarized photons and the interference between longitudinally and transversally polarized photons, since they give very small contribution [54]. As usual, we also do not take into account an emission of the final large- p_T photon directly from the electron [55].

The results presented in next sections are obtained in NLO QCD with use of the GRV set of parametrizations with $\mu = E_T^\gamma$ and $N_f = 4$ unless explicitly stated otherwise.

6 Results for the $ep \rightarrow e\gamma X$ process

The comparison with the ZEUS Collaboration data [8] for the photoproduction of isolated photons have been discussed in details in [2]. Recently a new preliminary data have been presented by the H1 Collaboration [10]. For a comparison with these data, we apply kinematic cuts used in [10], namely the fraction of the electron energy transferred to the photon is restricted to the range $0.2 < y < 0.7$, and the final photon rapidity and transverse energy are taken in the limits $-1 < \eta_\gamma < 0.9$ and $5 < E_T^\gamma < 10$ GeV, respectively.

In fig. 3 the differential cross sections $d\sigma/dE_T^\gamma$ and $d\sigma/d\eta_\gamma$ are shown. Our exact predictions (solid lines) are compared with the predictions obtained in the small cone approximation (dashed lines) discussed in our previous paper [2]. The differences do

not exceed 2%, so the small cone approximation works very well, despite the fact that the isolation cone of radius $R = 1$ is not a small one.

The predictions are in good agreement with the H1 preliminary data [10] (not shown) for both $d\sigma/dE_T^\gamma$ and $d\sigma/d\eta_\gamma$ distributions with exception of one experimental point at $\eta_\gamma > 0.58$, which lies below the predictions.

7 Results for the $ep \rightarrow e\gamma \text{ jet } X$ process

There are two publications of the ZEUS Collaboration presenting results of measurements of the isolated photon plus jet photoproduction at the HERA Collider [6, 9]. In the first paper [6] the total cross section integrated over some kinematic range is given. The aim of the second one [9] was to study transverse momentum of partons in the proton, and no data for cross sections were presented (although some data for distributions of events, not corrected for the detector effects, were shown).

In the new paper of the H1 Collaboration [10], the preliminary photoproduction data are presented for various differential cross sections of both $ep \rightarrow e\gamma X$ (considered above in sec. 6) and $ep \rightarrow e\gamma \text{ jet } X$ processes.

As in sec. 6, we impose kinematic limits used in the H1 analysis [10]. The cross sections are integrated over $0.2 < y < 0.7$, and $-1 < \eta_\gamma < 0.9$ and/or $5 < E_T^\gamma < 10$ GeV with the jet rapidity and jet transverse energy in the range $-1 < \eta_{jet} < 2.3$ and $4.5 \text{ GeV} < E_T^{jet}$, respectively. If two jets are found with the above parameters, that with higher E_T^{jet} is taken.

7.1 Theoretical uncertainties

As it is discussed in details in [28], the symmetric cuts for the photon and the jet transverse energy leads to unphysical results in next-to-leading or higher orders of calculations. This effect is shown in fig. 4a, where the LO and NLO predictions as a function of the photon transverse energy are shown in the E_T^γ -range wider than the range considered by the H1 Collaboration. At E_T^γ values close to the minimal jet transverse energy, $E_{T,min}^{jet} = 4.5$ GeV, the NLO differential cross section has a discontinuity: for $(E_T^\gamma)_- \rightarrow 4.5$ GeV it has a strong maximum, and a minimum for $(E_T^\gamma)_+ \rightarrow 4.5$ GeV. In the minimum the value of the cross section is even negative. This unphysical fluctuation is not present in the LO calculation.

An integration of the differential cross section over the photon transverse energy higher than the minimal jet transverse energy, $E_T^\gamma \geq E_{T,min}^{jet}$, leads to underestimated predictions in NLO. However numerically this effect is not very important.

To avoid theoretical instabilities, one can consider a cross section averaged over some E_T^γ -bins, see fig. 4b. Note, that the NLO predictions are well defined if one takes the cross section integrated/averaged over E_T^γ from $E_{T,min}^{jet} - \Delta$ to $E_{T,min}^{jet} + \Delta$, if Δ is sufficiently large, say $\Delta > 0.3$ GeV. So, the bins of a length 1 GeV presented in fig. 4b are large enough to avoid errors due to the symmetric cuts.

The cross section for $E_T^\gamma < E_{T,min}^{jet}$ is dominated by the NLO corrections, since the

LO contribution is suppressed by the E_T^{jet} -cut ($4.5 \text{ GeV} < E_T^{jet}$) and by the isolation requirement (sec. 3). We checked that the dependence on the renormalization/factorization scale, μ , is not strong: variations of μ from E_T^γ to $E_T^\gamma/2$ or $2E_T^\gamma$ lead to changes of the cross section less than 3% for $E_T^\gamma < E_{T,min}^{jet}$ and up to 5% for $E_T^\gamma > E_{T,min}^{jet}$.

The NLO predictions for various μ , and the LO predictions are also shown in fig. 5. In each presented here bin the dependence on the choice of μ is less than $\pm 5\%$ for both E_T^{jet} and η_{jet} distributions. The cross section is suppressed for E_T^{jet} close to or higher than the maximal transverse energy of the photon, $E_{T,max}^\gamma = 10 \text{ GeV}$. At negative η_{jet} the LO predictions are higher by 14%, and at positive η_{jet} they are lower than the NLO ones by 16-27%.

Since for $E_T^\gamma > E_{T,min}^{jet}$ the difference between LO and NLO is not larger than 27% and the variation of NLO results due to the variation of the μ scale is small, up to 5%, the calculation is stable, and one can expect that the QCD corrections of higher orders are not sizable. On the other hand, for $E_T^\gamma < E_{T,min}^{jet}$ the NLO corrections constitute almost 100% of the cross section, and the corrections of higher orders may change predictions.

In fig. 6 the results obtained using different parton densities in the proton are shown. The predictions of CTEQ6 (NLO) [47] are 6% higher than the predictions of MRST2002 (NLO) [46]. The GRV (NLO) [43] densities give results higher than MRST2002 by 5-7% at negative η_γ , and 3-5% at positive η_γ . Differences between CTEQ6 and GRV do not exceed 4%.

The comparison between different parton densities in the photon is shown in fig. 7 for the x_γ^{obs} distribution, where x_γ^{obs} is defined as

$$x_\gamma^{obs} = (E_T^{jet} e^{-\eta^{jet}} + E_T^\gamma e^{-\eta^\gamma}) / 2yE_e. \quad (19)$$

The GS (NLO) parametrization [51] give predictions lower than GRV (NLO) [44] by 20-36% for $x_\gamma^{obs} < 0.9$. This large difference is due to the charm threshold assumed in the GS parametrization at large scale, $\mu^2 = 50 \text{ GeV}^2$, much higher than thresholds in other considered herein parametrizations [2]. The results obtained with use of AFG (NLO) [48] and AFG02 (NLO) [49] are very similar, and only the latter is shown in fig. 7. It gives predictions up to 15% lower than GRV for $x_\gamma^{obs} < 0.9$. At large- x_γ^{obs} region, $x_\gamma^{obs} > 0.9$, the cross section is dominated by the contribution of processes with direct initial photons, and the differences between predictions of various parametrizations are small. For the total cross section integrated over all x_γ^{obs} values the difference between GRV and AFG02 (GS) is 4% (16%).

We have also compared predictions of GRV (LO) [44] and the new CJKL (LO) [52] parton densities in the photon, as well as predictions of DO (LO) [15], GRV (NLO) [45] and BFG (NLO) [53] fragmentation functions. The total LO cross section (within the kinematic range considered by the H1 Collaboration) for the GRV (LO) parametrization is higher than for CJKL (LO) by 3%. The isolation requirement reduce the contribution of processes involving the resolved final photon [2], so the dependence on the choice of fragmentation functions is weak, even if the fragmentation functions differ considerably from one another. The total cross sections obtained with DO and BFG (set I and set II) are lower than the predictions of GRV by 2% and 4%, respectively.

The GRV distributions for the proton, photon and fragmentation have been used as a reference, and each time only one parametrization has been changed for a comparison. The differences observed in the total cross section are not large (with an exception of the GS densities, which give predictions considerably lower than the other densities in the photon due to the specific treatment of the charm contribution). However, the differences can be larger if one changes simultaneously all the used distributions. For instance predictions of the MRST, AFG02 and BFG set are lower than the GRV predictions by about 11% .

7.2 Comparing with H1 preliminary data and with FGH predictions

The predictions shown in figs. 4-7 are in reasonable agreement with the preliminary data of the H1 Collaboration (not shown), although some considerable differences are present, especially for E_T^γ values below 6.7 GeV and for negative η_{jet} .

For $5 < E_T^\gamma < 6.7$ GeV and for $\eta_{jet} < -0.3$ the NLO result are higher than the measured cross section by two standard deviations. Sizable differences are also seen for positive η_γ values. In these kinematic ranges the predictions are in good agreement with the preliminary data, if one takes the number of active flavours $N_f = 3$ instead of $N_f = 4$ ³, but the scale $\mu = E_T^\gamma$, for E_T^γ above 5 GeV, seems to be too large to neglect the charm contribution.

Now, we make short comparison with the NLO predictions of Fontannaz, Guillet and Heinrich (FGH) [28] presented in [10]. The FGH calculation take into account the QCD corrections to the resolved-photon processes, which are not included in the calculation presented herein (see sec. 2 and ref. [2]). They also use parton parametrizations different than the GRV ones used by us.

In the considered kinematic range the total cross section of FGH is about 6% lower than our predictions. However differences are larger for the differential cross sections. For example, the FGH cross sections are lower by about 20% for $d\sigma/dE_T^\gamma$ and $d\sigma/d\eta^{jet}$ at $E_T^\gamma < 6.7$ GeV and $\eta^{jet} < -0.3$, respectively, and they give better agreement with the data. On the other hand, our predictions for $d\sigma/d\eta^{jet}$ ($d\sigma/dx_\gamma^{obs}$) slightly better describes the data at $\eta_{jet} > 1.6$ ($0.25 < x_\gamma^{obs} < 0.5$), where FGH predictions are about 45% (13%) higher than ours. In other kinematic ranges the differences between calculations are not larger than $\pm 15\%$ (usually below 10%), and both calculations lead to a similar description of the preliminary H1 data, although the $d\sigma/dE_T^{jet}$ distribution of FGH is a bit more flat and more consistent with data in shape.

³The previous comparison with the ZEUS data [8] for the $ep \rightarrow e\gamma X$ reaction led to opposite conclusions: the predictions for $N_f = 3$ were too low in each kinematic range and better agreement with data was observed for $N_f = 4$ and $N_f = 5$ [2].

8 Summary

We presented the results of the NLO calculation of the cross section for the photoproduction of the prompt photon and prompt photon plus jet at the ep collider DESY HERA.

A new exact calculation for the prompt photon production was performed. We found that the predictions agree within 2% with the results obtained in the small cone approximation used in our previous analysis [2].

The main aim of this paper was a detailed analysis of the prompt photon plus jet production in NLO. (In the previous analysis [2] we presented only the LO predictions.) The dependence on the choice of parton distribution functions was found to be of order 10%. The uncertainties due to the variation of the renormalization/factorization scale are of order $\pm 5\%$, and it may indicate that the corrections of higher orders are small. But for relatively low E_T^γ , $E_T^\gamma < E_{T,min}^{jet}$, the NLO corrections are very large while the LO contribution is suppressed, and we expect that in this region the corrections of higher orders could change the predictions.

Our predictions are in reasonably agreement with the H1 preliminary data [10], nevertheless in some kinematic ranges there are discrepancies up to two standard deviations.

Differences between our predictions and the predictions of Fontannaz, Guillet and Heinrich [28] presented in [10] are usually below 10%, but in some kinematic limits they are larger. The largest differences, up to 45% at large η_{jet} , are seen for the $d\sigma/d\eta_{jet}$ distribution. The experimental errors are too large to conclude which calculation gives better description of the H1 preliminary data.

Acknowledgments

We would like to thank S. Chekanov from the ZEUS Collaboration and J. Gayler from the H1 Collaboration for helpful discussions. We are also grateful to M. Fontannaz for providing fortran subroutines computing the AFG, AFG02 and BFG parton distributions. This work was partly supported by the European Community's Human Potential Programme under contract HPRN-CT-2002-00311 EURIDICE.

Appendix

A The notation

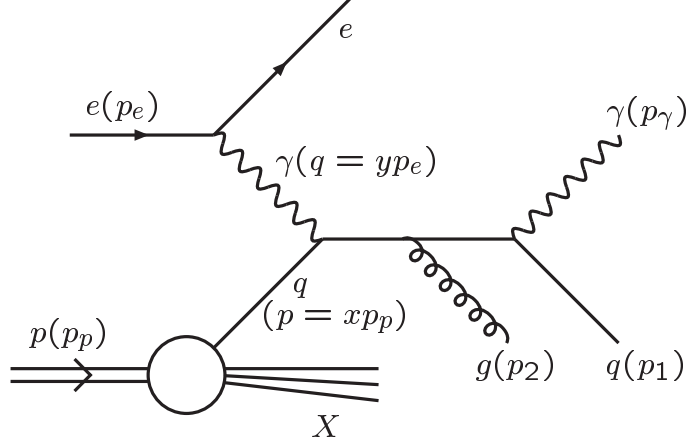


Figure 2: An example of the $2 \rightarrow 3$ NLO process. The omission of the final gluon gives the lowest order Born diagram ($\gamma q \rightarrow \gamma q$).

Here we introduce the notation which is used in Appendix B and in sec. 4. There are two kinds of $2 \rightarrow 3$ partonic processes:

$$\gamma(q) + q(p) \rightarrow \gamma(p_\gamma) + q(p_1) + g(p_2) \quad (\text{see fig. 2}), \quad (20)$$

and

$$\gamma(q) + g(p) \rightarrow \gamma(p_\gamma) + q(p_1) + \bar{q}(p_2). \quad (21)$$

The four-momenta of particles contributing to the processes are given in brackets. Let us define variables v and w :

$$v = 1 + t/s \quad , \quad w = -u/(t + s), \quad (22)$$

where

$$s = (q + p)^2 \quad , \quad t = (q - p_\gamma)^2 \quad \text{and} \quad u = (p - p_\gamma)^2. \quad (23)$$

The v and w variables are in the range $0 < v < 1$ and $0 < w < 1$. Note, that for massless particles $(p_1 + p_2)^2 = sv(1 - w)$, and in the limit $(p_1 + p_2)^2 \rightarrow 0$ one obtains $w \rightarrow 1$ (v can not be too low, since the final photon has large transverse momentum). For the $2 \rightarrow 2$ processes $w = 1$ by definition.

B Cross sections of $2 \rightarrow 3$ processes for collinear configurations

In this Appendix we have collected analytical formulae for the QCD corrections to the Born process in the regions of the phase space labeled as parts 2, 3 and 4 (sec. 4). The formulae are derived with an assumption that parameter θ_{cut} (R_{cut}) is small, $0 < \theta_{cut} \ll 1$ ($0 < R_{cut} \ll 1$), and all terms of order $\mathcal{O}(\theta_{cut}^n)$ ($\mathcal{O}(R_{cut}^n)$) are neglected for $n \geq 1$. All the collinear singularities are factorized into appropriate parton distributions with use of the dimensional regularization.

The QCD corrections to the Born process have contributions from all parts of the phase space:

$$E_\gamma \frac{d\sigma^{\gamma p \rightarrow \gamma(jet)X}}{d^3p_\gamma} \Big|_{QCD \text{ corr}} = \sum_{i=1,2,3,4,5} E_\gamma \frac{d\sigma_i^{\gamma p \rightarrow \gamma(jet)X}}{d^3p_\gamma} \Big|_{QCD \text{ corr}}. \quad (24)$$

As explained in sec. 4, in parts 1 and 5 we use formulae taken from ref. [17]. The corresponding cross sections for the $\gamma p \rightarrow \gamma(jet)X$ reaction in parts 2, 3 and 4 consists of the contributions of the $\gamma q \rightarrow \gamma qg$ and $\gamma g \rightarrow \gamma q\bar{q}$ processes:

$$\begin{aligned} E_\gamma \frac{d\sigma_i^{\gamma p \rightarrow \gamma(jet)X}}{d^3p_\gamma} \Big|_{QCD \text{ corr.}} &= \\ &= \int_0^1 \theta(s+t+u) \sum_{q=u,\bar{u} \dots}^{2N_f} \left[f_{q/p}(x) E_\gamma \frac{d\sigma_i^{\gamma q \rightarrow \gamma qg}}{d^3p_\gamma} + f_{g/p}(x) E_\gamma \frac{d\sigma_i^{\gamma g \rightarrow \gamma q\bar{q}}}{d^3p_\gamma} \right] dx, \end{aligned} \quad (25)$$

where $i = 2, 3$ or 4 and the summation runs over all quarks' and antiquarks' flavours. We include $2N_f$ flavours in $d\sigma_{2,3,4}^{\gamma g \rightarrow \gamma q\bar{q}}$, since there are N_f possible pairs $q\bar{q}$, and in each pair the quark or antiquark can be collinear to the initial electron, initial proton or to the final photon. The expressions for the partonic cross sections in parts 2, 3 and 4 are:

$$E_\gamma \frac{d\sigma_2^{\gamma q \rightarrow \gamma qg}}{d^3p_\gamma} = \frac{1}{vws^2} \frac{\alpha}{2\pi} P_{\gamma \rightarrow q\bar{q}}(w, y E_e \theta_{cut}) |\bar{M}^{q\bar{q} \rightarrow \gamma g}(v)|^2, \quad (26)$$

$$E_\gamma \frac{d\sigma_2^{\gamma g \rightarrow \gamma q\bar{q}}}{d^3p_\gamma} = \frac{1}{vws^2} \frac{\alpha}{2\pi} P_{\gamma \rightarrow q\bar{q}}(w, y E_e \theta_{cut}) |\bar{M}^{qg \rightarrow \gamma q}(v)|^2, \quad (27)$$

$$E_\gamma \frac{d\sigma_3^{\gamma q \rightarrow \gamma qg}}{d^3p_\gamma} = \frac{1}{(1-v)s^2} \frac{\alpha_S}{2\pi} P_{q \rightarrow qg}\left(\frac{1-v}{1-vw}, x E_p \theta_{cut}\right) |\bar{M}^{\gamma q \rightarrow \gamma q}(vw)|^2, \quad (28)$$

$$E_\gamma \frac{d\sigma_3^{\gamma g \rightarrow \gamma q\bar{q}}}{d^3p_\gamma} = \frac{1}{(1-v)s^2} \frac{\alpha_S}{2\pi} P_{g \rightarrow q\bar{q}}\left(\frac{1-v}{1-vw}, x E_p \theta_{cut}\right) |\bar{M}^{\gamma q \rightarrow \gamma q}(vw)|^2, \quad (29)$$

$$\begin{aligned}
E_\gamma \frac{d\sigma_4^{\gamma q \rightarrow \gamma qg}}{d^3p_\gamma} &= \\
&= \frac{1}{(1-v+vw)s^2} \frac{\alpha}{2\pi} P_{q \rightarrow \gamma q}(1-v+vw, E_T^\gamma R_{cut}) |\bar{M}^{\gamma q \rightarrow qg}(\frac{vw}{1-v+vw})|^2, \quad (30)
\end{aligned}$$

$$\begin{aligned}
E_\gamma \frac{d\sigma_4^{\gamma g \rightarrow \gamma q\bar{q}}}{d^3p_\gamma} &= \\
&= \frac{1}{(1-v+vw)s^2} \frac{\alpha}{2\pi} P_{q \rightarrow \gamma q}(1-v+vw, E_T^\gamma R_{cut}) |\bar{M}^{\gamma g \rightarrow q\bar{q}}(\frac{vw}{1-v+vw})|^2, \quad (31)
\end{aligned}$$

where we have used the notation:

$$P_{g \rightarrow q\bar{q}}(z, E) = \frac{1}{2} \left\{ [z^2 + (1-z)^2] \ln \frac{(1-z)^2 E^2}{\mu^2} + 1 \right\}, \quad (32)$$

$$P_{\gamma \rightarrow q\bar{q}}(z, E) = 2N_C e_q^2 P_{g \rightarrow q\bar{q}}(z, E), \quad (33)$$

$$P_{q \rightarrow qg}(z, E) = C_F \left\{ \frac{1+z^2}{1-z} \ln \frac{(1-z)^2 E^2}{\mu^2} + 1 - z \right\}, \quad (34)$$

$$P_{q \rightarrow \gamma q}(z, E) = e_q^2 \left\{ \frac{1+(1-z)^2}{z} \ln \frac{(1-z)^2 E^2}{\mu^2} + z \right\}, \quad (35)$$

$$|\bar{M}^{\gamma g \rightarrow q\bar{q}}(v)|^2 = \alpha \alpha_S e_q^2 \frac{v^2 + (1-v)^2}{v(1-v)}, \quad (36)$$

$$|\bar{M}^{q\bar{q} \rightarrow \gamma g}(v)|^2 = \frac{2C_F}{N_C} |\bar{M}^{\gamma g \rightarrow q\bar{q}}(v)|^2, \quad (37)$$

$$|\bar{M}^{\gamma q \rightarrow \gamma q}(v)|^2 = 2\alpha^2 e_q^4 \frac{1+v^2}{v}, \quad (38)$$

$$|\bar{M}^{\gamma q \rightarrow qg}(v)|^2 = \frac{C_F}{e_q^2} \frac{\alpha_S}{\alpha} |\bar{M}^{\gamma q \rightarrow \gamma q}(1-v)|^2, \quad (39)$$

$$|\bar{M}^{qg \rightarrow \gamma q}(v)|^2 = \frac{1}{2N_C e_q^2} \frac{\alpha_S}{\alpha} |\bar{M}^{\gamma q \rightarrow \gamma q}(1-v)|^2. \quad (40)$$

References

- [1] M. Krawczyk and A. Zembrzuski, in: A. Astbury, D. Axen, J. Robinson (Eds.), Proceedings of the 29th Int. Conference on High Energy Physics, ICHEP'98, Vancouver, Canada, July 1998, World Scientific, 1999, p.895, arXiv:hep-ph/9810253.
- [2] M. Krawczyk and A. Zembrzuski, Phys. Rev. D **64** (2001) 114017.
- [3] M. Klasen, Rev. Mod. Phys. **74** (2002) 1221.
- [4] M. Krawczyk, A. Zembrzuski and M. Staszal, Phys. Rept. **345** (2001) 265
- [5] R. Nisius, Phys. Rep. **332** (2000) 165.
- [6] J. Breitweg *et al.* [ZEUS Collaboration], Phys. Lett. B **413** (1997) 201.
- [7] ZEUS Collaboration, prepared for 29th Int. Conference on High Energy Physics (ICHEP 98), Vancouver, Canada, July 1998.
- [8] J. Breitweg *et al.* [ZEUS Collaboration], Phys. Lett. B **472** (2000) 175.
- [9] S. Chekanov *et al.* [ZEUS Collaboration], Phys. Lett. B **511** (2001) 19.
- [10] H1 Collaboration, submitted to the Int. Europhysics Conference on High Energy Physics, EPS03, July 2003, Aachen (Abstract 093), and to the XXI Int. Symposium on Lepton and Photon Interactions, LP03, August 2003, Fermilab.
- [11] J. D. Bjorken and E. A. Paschos, Phys. Rev. **185** (1969) 1975.
- [12] T. s. Tu and C. m. Wu, Nucl. Phys. B **156** (1979) 493.
- [13] K. Iguchi and A. Niegawa, Prog. Theor. Phys. **64** (1980) 1093; Z. Phys. C **9** (1981) 135.
- [14] M. Fontannaz and D. Schiff, Z. Phys. C **14** (1982) 151.
- [15] D. W. Duke and J. F. Owens, Phys. Rev. D **26** (1982) 1600 [Erratum-ibid **28** (1983) 1227].
- [16] A. Czechowski, M. Krawczyk, T. Hofmohl, A. Jacholkowska and M. Gorski, Z. Phys. C **19** (1983) 95.
- [17] P. Aurenche, A. Douiri, R. Baier, M. Fontannaz and D. Schiff, Z. Phys. C **24** (1984) 309.
- [18] A. C. Bawa and W. J. Stirling, J. Phys. G **14** (1988) 1353.
- [19] M. Krawczyk, Acta Physica Polonica B **21** (1990) 999.
- [20] A. C. Bawa, M. Krawczyk and W. J. Stirling, Z. Phys. C **50** (1991) 293.

- [21] A. C. Bawa and M. Krawczyk, Phys. Lett. B **262** (1991) 492.
- [22] A. C. Bawa and M. Krawczyk, Proceedings “Physics at HERA”, Hamburg 1991, p. 579, IFT-17-91.
- [23] P. Aurenche, P. Chiappetta, M. Fontannaz, J. P. Guillet and E. Pilon, Z. Phys. C **56** (1992) 589.
- [24] L. E. Gordon and J. K. Storrow, Z. Phys. C **63** (1994) 581.
- [25] L. E. Gordon and W. Vogelsang, Phys. Rev. D **52** (1995) 58; hep-ph/9606457.
- [26] M. Fontannaz, J. P. Guillet and G. Heinrich, Eur. Phys. J. C **21** (2001) 303
- [27] L. E. Gordon, Phys. Rev. D **57** (1998) 235.
- [28] M. Fontannaz, J. P. Guillet and G. Heinrich, Eur. Phys. J. C **22** (2001) 303.
- [29] G. Kramer, D. Michelsen and H. Spiesberger, Eur. Phys. J. C **5** (1998) 293; A. Gehrmann-De Ridder, G. Kramer and H. Spiesberger, Phys. Lett. B **459** (1999) 271; Eur. Phys. J. C **11** (1999) 137; Nucl. Phys. B **578** (2000) 326.
- [30] H1 Collaboration, Abstract 265, submitted to the Int. Europhysics Conference on High Energy Physics, HEP97, Jerusalem, Israel, August 1997.
- [31] P.J. Bussey, talk given at the 9th Int. Workshop on Deep Inelastic Scattering, Bologna, Italy, 27 April - 1 May 2001; see also arXiv:hep-ex/0107063.
- [32] T. F. Walsh and P. M. Zerwas, Phys. Lett. B **44** (1973) 195; E. Witten, Nucl. Phys. B **120** (1977) 189; W. A. Bardeen and A. J. Buras, Phys. Rev. D **20** (1979) 166 [Erratum-ibid. D **21** (1980) 2041].
- [33] R. J. DeWitt, L. M. Jones, J. D. Sullivan, D. E. Willen and H. W. Wyld, Phys. Rev. D **19** (1979) 2046 [Erratum-ibid. D **20** (1979) 1751].
- [34] J. Chýla, JHEP **0004** (2000) 007; arXiv:hep-ph/9811455; arXiv:hep-ph/0010140; arXiv:hep-ph/0010309.
- [35] B. L. Combridge, Nucl. Phys. B **174** (1980) 243.
- [36] C. F. von Weizsäcker, Z. Phys. **88** (1934) 612.
- [37] E. J. Williams, Phys. Rev. **45** (1934) 729.
- [38] V. M. Budnev, I. F. Ginzburg, G. V. Meledin and V. G. Serbo, Phys. Rep. **15** (1975) 181.
- [39] S. Frixione, M. L. Mangano, P. Nason and G. Ridolfi, Phys. Lett. B **319** (1993) 339.

- [40] S. D. Ellis and D. E. Soper, Phys. Rev. D **48** (1993) 3160; S. Catani, Y. L. Dokshitzer, M. H. Seymour and B. R. Webber, Nucl. Phys. B **406** (1993) 187.
- [41] J. Żochowski, “*The corrections of order α_S in Deep Inelastic Compton Scattering*”, *MS Thesis, 1992*.
- [42] S. Bethke, arXiv:hep-ex/0211012; J. Phys. G **26** (2000) R27.
- [43] M. Glück, E. Reya and A. Vogt, Z. Phys. C **67** (1995) 433.
- [44] M. Glück, E. Reya and A. Vogt, Phys. Rev. D **45** (1992) 3986; Phys. Rev. D **46** (1992) 1973.
- [45] M. Glück, E. Reya and A. Vogt, Phys. Rev. D **48** (1993) 116.
- [46] A. D. Martin, R. G. Roberts, W. J. Stirling and R. S. Thorne, Eur. Phys. J. C **28** (2003) 455.
- [47] J. Pumplin, D. R. Stump, J. Huston, H. L. Lai, P. Nadolsky and W. K. Tung, JHEP **0207** (2002) 012.
- [48] P. Aurenche, J. P. Guillet and M. Fontannaz, Z. Phys. C **64** (1994) 621.
- [49] P. Aurenche, J. P. Guillet and M. Fontannaz, 2002. This is a new version of the AFG parametrization [48]. Some informations about it can be found in the ref. [50].
- [50] M. Fontannaz, J. P. Guillet and G. Heinrich, Eur. Phys. J. C **26** (2002) 209.
- [51] L. E. Gordon and J. K. Storrow, Nucl. Phys. B **489** (1997) 405.
- [52] F. Cornet, P. Jankowski, M. Krawczyk and A. Lorca, Phys. Rev. D **68** (2003) 014010.
- [53] L. Bourhis, M. Fontannaz and J. P. Guillet, Eur. Phys. J. C **2** (1998) 529.
- [54] U. Jezuita-Dąbrowska and M. Krawczyk, Acta Phys. Polon. B **34** (2003) 3133; arXiv:hep-ph/0211112.
- [55] U. Jezuita-Dąbrowska, “*The polarization states of the virtual photon in $ep \rightarrow e\gamma X$ at the HERA collider*”, *MS Thesis, 1999*.

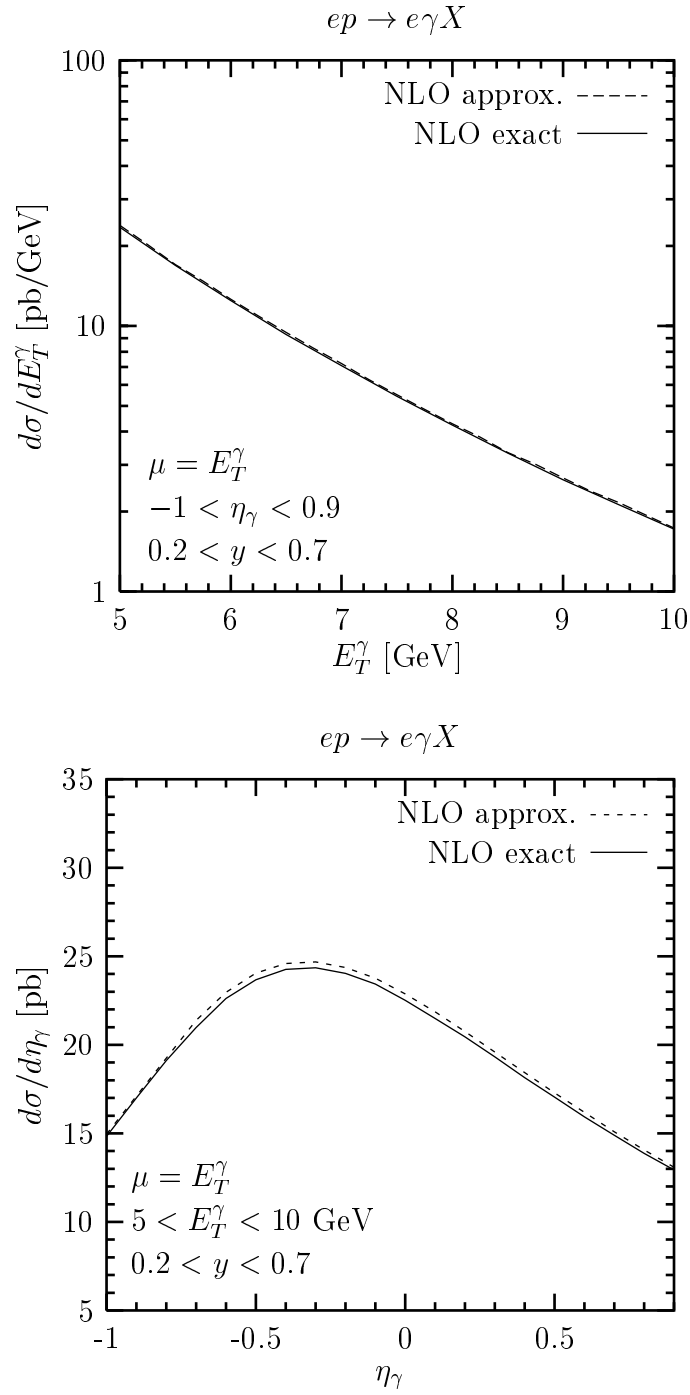


Figure 3: The comparison between predictions obtained in the small cone approximation (dashed line) and exact ones (solid line) for the $ep \rightarrow e\gamma X$ photoproduction. The $d\sigma/dE_T^\gamma$ (a) and $d\sigma/d\eta_\gamma$ (b) cross sections are shown.

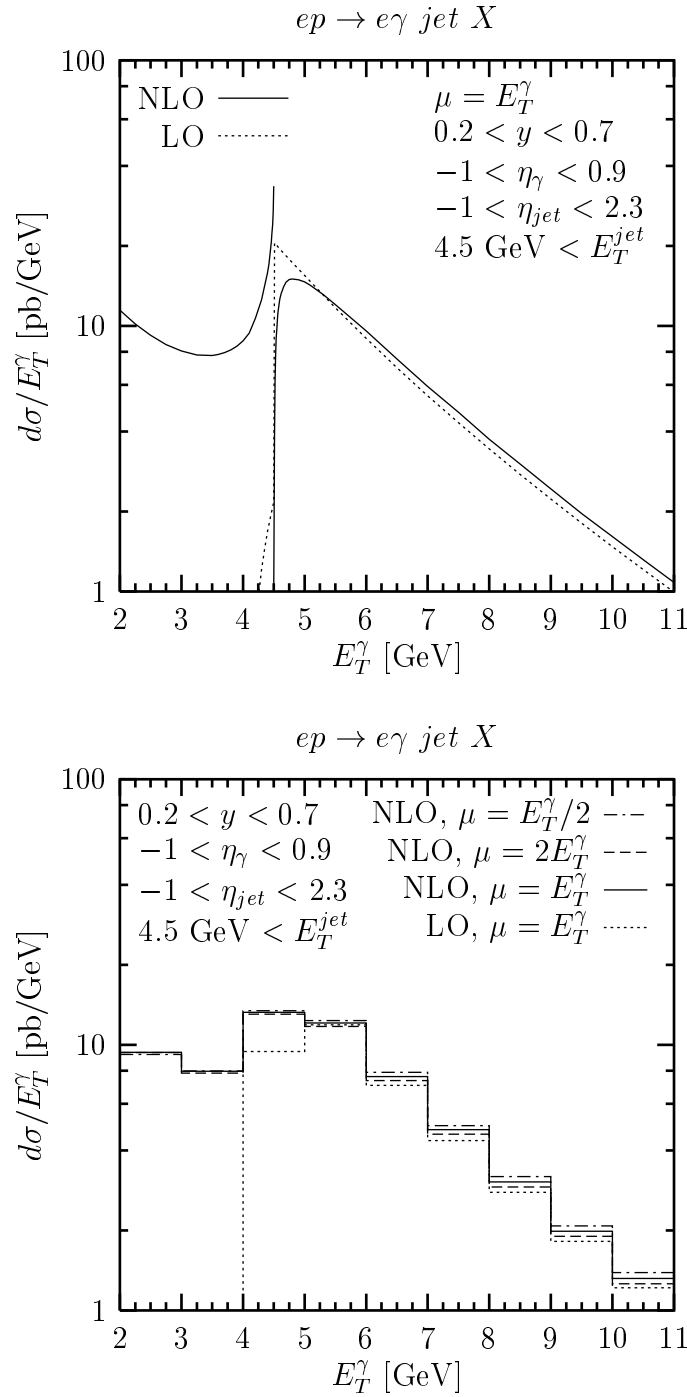


Figure 4: The differential cross section $d\sigma/dE_T^\gamma$ (a) and the differential cross section $d\sigma/dE_T^\gamma$ averaged over E_T^γ -bins (b) for the $ep \rightarrow e\gamma \text{ jet } X$ process. The NLO predictions for $E_T^\gamma = \mu$ (a) and for μ between $E_T^\gamma/2$ and $2E_T^\gamma$ (b) are shown together with the LO predictions.

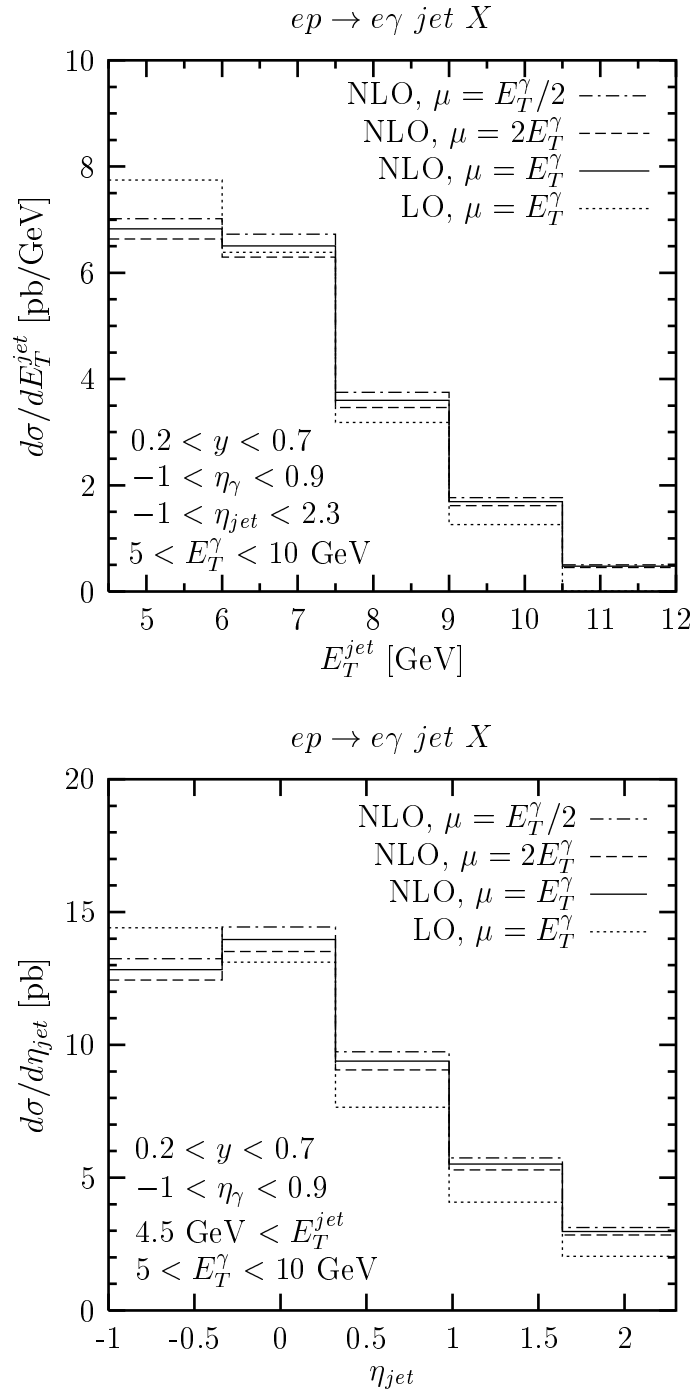


Figure 5: The NLO predictions with μ between $E_T^\gamma/2$ and $2E_T^\gamma$ and the LO predictions for $d\sigma/dE_T^{jet}$ (a) and $d\sigma/d\eta_{jet}$ (b) distributions.

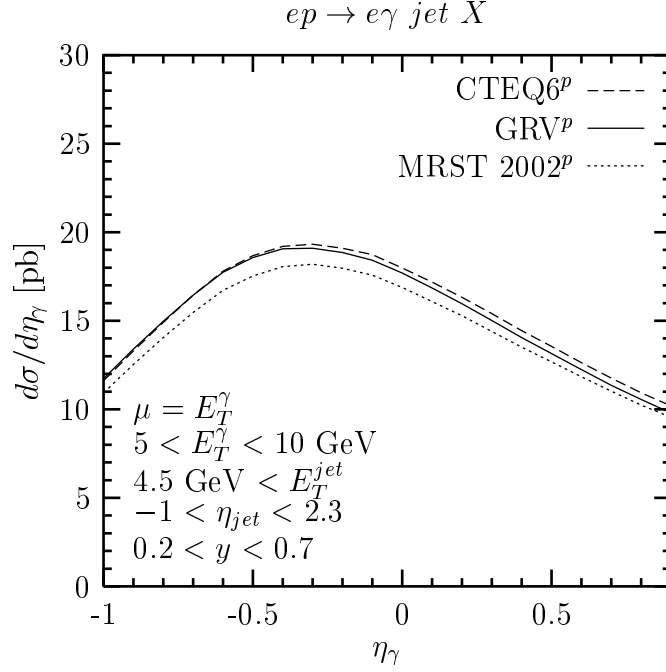


Figure 6: The differential cross section $d\sigma/d\eta_\gamma$ for GRV [43], MRST2002 [46] and CTEQ6 [47] parton distributions in the proton.

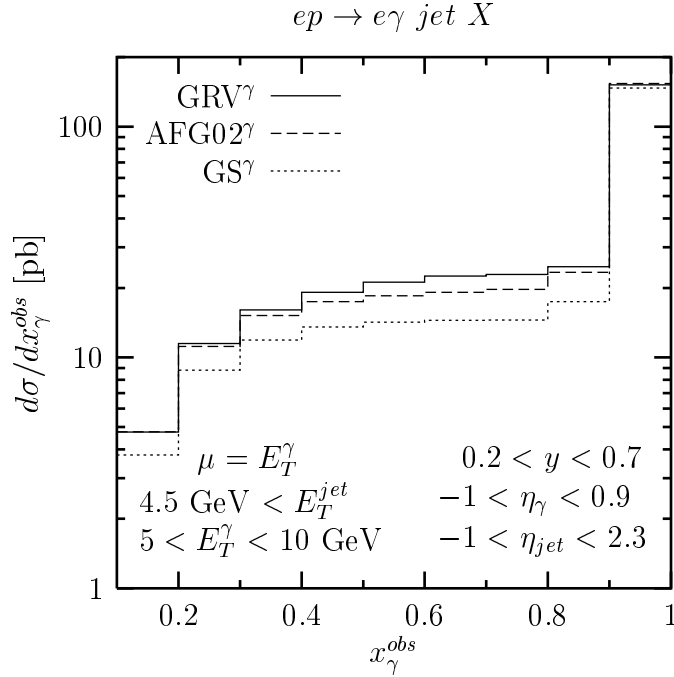


Figure 7: The differential cross section $d\sigma/dx_\gamma^{obs}$ for GRV [44], GS [51] and AFG02 [49] parton distributions in the photon.